Astron. Astrophys. 358, 208–220 (2000)

ASTRONOMY AND ASTROPHYSICS

The circumstellar structure of the Be shell star ϕ Per*

I. Data analysis

S. Štefl[1], **W. Hummel**[2], **and Th. Rivinius**[3,4]

[1] Astronomical Institute, Academy of Sciences of the Czech Republic, 25165 Ondřejov (sstefl@sunstel.asu.cas.cz)
[2] Institut für Astronomie und Astrophysik und Universitätssternwarte München, Scheinerstrasse 1, 81673 München, Germany (hummel@bigbang.usm.uni-muenchen.de)
[3] European Southern Observatory, Karl-Schwarzschild-Strasse 2, 85748 Garching bei München (triviniu@eso.org)
[4] Landessternwarte Königstuhl, 69117 Heidelberg, Germany

Received 19 February 2000 / Accepted 14 March 2000

Abstract. We present new phase resolved observations of emission lines of the Be binary ϕ Per.

Analyzing the orbital phase variations in the He I emission features we find strong arguments that the feature as a whole originates in the outer parts of the disk around the primary star. In addition to the He I 6678 and 5876 lines, the emission features with orbital phase variations were detected in three more He I lines. The observations are in agreement with the scenario of Poeckert and others, in which the outer parts of an axisymmetric disk are illuminated by the radiation of the secondary. The observations after 1996 are consistent with a growing global density inhomogeneity in the circumprimary disk as it occurs in disks of single Be stars. The combination of the illumination effect and the increasing density inhomogeneity make ϕ Per an ideal laboratory to study density perturbations of circumstellar disks of Be stars in more detail.

Key words: line: profiles – radiative transfer – stars: binaries: general – stars: circumstellar matter – stars: emission-line, Be – stars: individual: ϕ Per

1. Introduction

ϕ Per (HR 496, HD 10516) is a spectroscopic binary with a period of $P \simeq 127$d (Ludendorff 1910). According to data from the Hipparcos satellite, it is at a distance of 220 ± 36 pc (Perryman 1997). Its optical component is a fast rotating Be shell star with MK=B0.5IV (Božić et al. 1995), $v \sin i = 450$ km s^{-1} (Poeckert 1981) and M_V = –3.11 $\pm$ 0.36 (Gies et al. 1998). The corresponding radius is 7 $R_\odot$ (Harmanec 1988). The secondary is known to be a sdO dwarf star with $T_{\rm eff} = 53\,000$ K (Gies et al. 1998) and $\log g = 4.2$. The latter authors derived the separation of the components $a = 232\ R_\odot$.

The current picture is that ϕ Per is a post-case C mass transfer system. The secondary is a bare stellar core stripped-down after an extensive mass transfer (see e.g. Vanbeveren et al. 1998).

An extended circumstellar disk is formed around the primary component. Its geometrical properties have been measured by combined interferometric and polarimetric observations (Quirrenbach et al. 1997). Using their angular diameter of the Hα emitting region and Hipparcos distance, the outer radius of the disk can be estimated as $\approx 63\ R_\odot$, what corresponds to about 9 radii of the primary Be star (Štefl 1999).

The full history of ϕ Per observations until 1995 was given by Božić et al. (1995).

The most impressive peculiarity of ϕ Per are the variations of the optical and UV spectral lines, giving rise to a more complex circumstellar structure than Keplerian disks generally do around most normal single Be stars. The spectral components previously identified in the optical spectrum are:

1. Broad stellar absorption profiles originating in the atmosphere of the primary.
2. H I, Fe II, and Si II emission lines of the common Be profile type, the radial velocities of which follow the B-type primary and which originate in its circumstellar disk.
3. Narrow He I shell absorption profiles with intensity maxima around superior conjunction of the primary, which follow the primary motion and which probably originate in the outer parts of the disk around the primary (Poeckert 1981). In some lines, the components appear only at superior conjunction. Also Fe IV lines observed in the UV region (Gies et al. 1998) may fall in this category.
4. A broad double-peak He II 4686 emission line, varying in anti-phase at a larger RV amplitude with respect to (1,2,3) and probably originating in a disk around the secondary. Narrow weak UV Fe V lines reported by Thaller et al. (1995) were also attributed to the secondary's atmosphere.

Send offprint requests to: S. Štefl

* Based on observations collected at the Ondřejov Observatory (of the Academy of Sciences of the Czech Republic), Heidelberg Observatory, German-Spanish Astronomical Center (DSAZ) - Calar Alto (operated by the Max-Plank-Institut für Astronomie Heidelberg jointly with the Spanish National Commission for Astronomy) and Observatoire de Haute-Provence (OHP; CNRS, France)

5. Weak narrow He I shell absorption, only appearing in phases near the two quadratures. Their RVs are consistent with the orbital velocity field of the secondary.
6. A complex emission structure seen in He I 6678 (Gies et al. 1993) and He I 5875 (Hummel & Vrancken 1995) varying in anti-phase with respect to the primary.

The origin of the last spectral component is still mysterious. Gies et al. (1993) proposed that the stronger component of the He I emission feature originates in the outer cooler part of the disk around the secondary, while the fainter emission component is formed either in a gas stream (from the secondary towards the primary) or in the outer parts of the disk around the primary. Božić et al. (1995) also found the He I 6678 emission feature, but advocated that it may be a double emission from a disk around the secondary. Hummel & Vrancken (1995) detected a similar emission component in He I 5876 (coincidentally at the phase of inferior conjunction of the primary) and proposed that the He I emission originates in the disk further than 7 R_* from the primary.

At variance to these suggestions, Suzuki et al. (1997) proposed that the Balmer emission originates in a disk around the primary and a ring around the whole binary system.

The generally accepted ephemeris by Božić et al. (1995) was derived from radial velocities of emission lines, measured in their wings. The authors identified the Balmer and metallic lines with the primary and peculiar He I emission component with the secondary star. They used the same values to derive the binary parameters. However, their velocity amplitudes are lower by $\approx$ 15–20 % and consequently their masses about two times higher than derived by Gies et al. (1998) from the UV absorption lines. For the reasons given further in this paper we prefer Gies' et al. solution with masses of 9.3 $\pm$0.3 $\mathrm{M}_\odot$ and $1.14 \pm 0.04\,\mathrm{M}_\odot$ for the primary and the secondary companion, respectively.

In this first paper of our study, we present the analysis of our new data. They enable us to analyze the spectra from the following aspects:

1. Variability on a time scale considerably longer than the orbital period.
2. Occurrence of individual peculiar features in different spectral lines.
3. Detailed phase variation of selected well monitored spectral lines. This way we can focus on the distribution of the emitting gas, location and kinematics of the He I 6678 emission feature and its modeling.

The third aspect forms the base for a more complete and physical modeling of the system to be presented in a forthcoming second paper.

In Sect. 2 we describe our new spectroscopic observations. The long term and orbital variations of different emission lines are discussed in Sect. 3, while Sect. 4 provides a detailed analysis of occurrence of the emission component in He I lines and of its phase variations in He I 6678. The consequences for the origin of the component and the whole model are discussed in Sect. 5.

To avoid any confusion in comparison of our results with previous studies, we note that Gies et al. (1993) and Thaller et al. (1995) used the ephemeris by Poeckert (1981), while Gies et al. (1998) and this study rely on the ephemeris by Božić et al. (1995). The major difference between the two is that Božić et al. (1995) define phase $0.^P0$ at the primary conjunction (primary is in front of the secondary, $\mathrm{RV}_{\mathrm{primary}} = 0$). It occurs at phase $0.^P46$ in the older ephemeris.

2. Observations and their reduction

2.1. Ondřejov observations

Altogether 82 spectra were obtained in the coudé focus of the Ondřejov 2m telescope in the period August 1993 - October 1999. We used the Reticon 1872 RF detector on loan from the Lick Observatory. The spectral coverage is 6290–6720 Å, linear dispersion 17 Å/mm, resolution about 0.214 Å/pixel and S/N mostly higher than 500. Typical exposure time was 30 - 40 minutes. The spectra were reduced in the standard way using the program SPEFO by J. Horn. In spite of lower spectral resolution, Reticon spectra do not suffer by any fringing and – also thanks to high S/N – are well suitable for a detailed study of line profile variations in the given spectral range.

Table 1 gives the summary of the observations.

2.2. Calar Alto, OHP observations

High-resolution observations of Hα, Fe II 5317 and He I 5876 emission lines have been obtained during several runs at the 2.2m telescope on Calar Alto (Coudé focus f/40 + CCD, $R = \lambda/\Delta\lambda = 45\,000$ at Hα, $R = 32\,000$ at He I 5876, and $R = 28\,000$ at Fe II 5317) and the 1.52m telescope of the Observatoire de Haute Provence (Coudé focus, Aurelie spectrograph + one-dimensional CCD (Barette Thomson), $R = 72\,000$ at Hα, $R = 51\,000$ at He I 5876, and $R = 44\,000$ at Fe II 5317) in context of a survey on the long-term variability of northern Be stars (Hummel & Vrancken 1995, 2000). The exposure times were between 15 and 45 minutes.

The data reduction includes correction for offset (read-out-noise), flat-field, wavelength calibration, terrestrial water vapor correction with a mask obtained from a bright O-type star and correction of the heliocentric velocity frame. Details can be found in Hummel & Vrancken (1995). Table 2 shows the log of observations.

2.3. HEROS *observations*

In 1998 we obtained additional spectra using the HEROS spectrograph during times ranging from January 12 to February 11 at the 72 cm Waltz reflector of the Landessternwarte Königstuhl and from August 4 to October 4 at the 1.23m telescope of the Calar Alto observatory. Table 3 gives the log of observations.

The fiber-linked echelle spectrograph HEROS (**H**eidelberg **E**xtended **R**ange **O**ptical **S**pectrograph, e.g. Kaufer 1998, Štefl & Rivinius 2000) uses a dichroic beam splitter to divide the light beam into two channels after the echelle grating. Each

Table 1. Observations obtained with the Ondřejov 2-m telescope. Heliocentric Julian date is calculated for mid-exposures, phase according to the ephemeris by Božić et al. (1995): P=126.6731, $T_0 = 2435046.73$, $K_1 = 10.4\,\mathrm{km\ s^{-1}}$. V_{orbit} is the radial velocity of the primary, $V_{\mathrm{He-em}}$ are the measured heliocentric radial velocities of the violet and red components of He I 6678. Their phase diagram is shown in Fig. 7, lower panel

JD −2 400 000	Frame No.	phase	V_{orbit} km s^{-1}	$V_{\mathrm{He-em}}$ km s^{-1}
49206.4721	2258	111.7819	10.19	−134 / -
49214.5395	2378	111.8455	8.59	−139 / -
49249.4681	2691	112.1213	−7.18	- / +88
49250.6224	2729	112.1304	−7.59	- / +91
49260.5348	2917	112.2086	−10.05	- / +109
49267.3840	2963	112.2627	−10.37	- / +110
49288.4357	3114	112.4289	−4.50	- / +99
49291.4302	3318	112.4525	−3.06	- / +68
49322.4418	3544	112.6973	9.83	−126 / -
49382.2694	3729	112.1697	−9.10	- / +94
49528.5476	5128	113.3244	−9.29	- / +107
49529.5498	5167	114.3323	−9.04	- / +112
49568.5191	5598	114.6400	8.01	−118 / -
49580.4856	5682	114.7344	10.35	−126 / -
49581.4817	5727	114.7423	10.39	−134 / -
49612.4680	5987	114.9869	0.86	−82 / -
49625.4460	6171	115.0894	−5.53	- / +79
49634.4406	6350	115.1604	−8.79	- / +91
49644.3283	6691	115.2384	−10.37	- / +103
49644.4805	6704	115.2396	−10.38	- / +107
49658.4058	6877	115.3496	−8.43	- / +105
49659.5219	6928	115.3584	−8.08	- / +106
49661.2888	6968	115.3723	−7.48	- / +102
49662.3221	6998	115.3805	−7.10	- / +100
49679.3209	7064	115.5147	0.95	−106 / +81
49915.4826	8531	117.3790	−7.17	- / +109
49918.5267	8570	117.4031	−5.96	- / +100
49930.4317	8761	117.4970	−0.20	−107 / +73
49932.4517	8808	117.5130	0.84	−118 / +40
49948.5115	8981	117.6398	8.00	−118 / -
49948.5275	8982	117.6399	8.00	−117 / -
49949.5119	9012	117.6477	8.32	−115 / -
49974.4946	9158	117.8449	8.61	−138 / -
49977.4687	9186	117.8684	7.66	−132 / -
49977.4857	9187	117.8685	7.65	−127 / -
49979.5073	9223	117.8845	6.91	−125 / -
50001.5890	9383	118.0588	−3.75	- / +58
50001.6145	9384	118.0590	−3.76	- / +54
50014.2831	9450	118.1590	−8.74	- / +87
50015.4090	9498	118.1679	−9.04	- / +91
50030.4105	9564	118.2863	−10.13	- / +109
50043.4553	9596	118.3893	−6.67	- / +104
50080.2587	9661	118.6798	9.40	−117 / -
50080.2951	9662	118.6801	9.41	−120 / -
50104.2618	9834	118.8693	7.62	−127 / -
50295.5556	11340	120.3794	−7.15	- / +100
50297.5009	11366	120.3948	−6.39	- / +100
50297.5169	11367	120.3949	−6.38	- / +101
50302.5447	11395	120.4346	−4.16	- / +96
50304.4159	11430	120.4494	−3.26	- / +85
50315.4958	11491	120.5369	2.38	−145 / +76
50315.5129	11492	120.5370	2.39	−128 / +81
50316.4869	11518	120.5447	2.88	−133 /+115
50365.3959	11681	120.9308	4.39	−125 / -
50410.4100	12124	121.2861	−10.13	- / +117
50413.2276	12140	121.3084	−9.71	- / +120
50439.2259	12219	121.5136	0.88	−119 / +85
50448.3172	12245	121.5854	5.31	−127 / -
50499.3582	12539	121.9883	0.77	−7 / -
50508.2743	12584	121.0587	−3.74	- / +52
50509.2469	12603	121.0664	−4.21	- / +76
50510.2989	12636	121.0747	−4.70	- / +67
50512.2711	12651	121.0903	−5.58	- / +79
51043.4282	13254	126.2834	−10.17	- / +129
51043.5911	13261	126.2847	−10.16	- / +130
51384.5482	14171	128.9763	1.55	- / +49
51388.4887	14211	129.0074	−0.48	- / +49
51391.4728	14280	129.0310	−2.01	- / +55
51416.5737	14616	129.2291	−10.31	- / +115
51416.6044	14617	129.2294	−10.31	- / +114
51430.5271	14702	129.3393	−8.81	- / +122
51430.5381	14703	129.3394	−8.81	- / +123
51430.5612	14704	129.3396	−8.80	- / +125
51431.4035	14718	129.3462	−8.56	- / +127
51431.4284	14719	129.3464	−8.55	- / +122
51432.6254	14772	129.3559	−8.19	- / +124
51435.5571	14858	129.3790	−7.17	- / +129
51435.5948	14860	129.3793	−7.16	- / +128
51436.6179	14883	129.3874	−6.77	- / +127
51443.6043	14914	129.4425	−3.68	- / +118
51464.5868	14990	129.6082	6.53	- / -
51470.5481	15042	129.6552	8.61	- / -

channel has its own cross-disperser, camera, and detector. The blue one covers the range from 3450 Å to 5560 Å, and the red one from 5820 Å to 8620 Å. The spectral resolving power in both channels is $\lambda/\Delta\lambda \approx 20\,000$. The link to the telescopes is provided by a 10 m long optical fiber.

The standard reduction, extraction, and visualization of the data is based on a customized version of the ESO-Midas echelle context and was described in detail by Stahl et al. (1995).

The typical S/N ratio of the spectra measured in the Hβ region is about 100.

3. Long-term vs. orbital spectral variations

In previous studies, all spectral variations were considered as orbital ones, and the parameters of the binary system were derived under this assumption. Although it is very probable that the orbital variations are dominant in the ϕ Per spectrum, a better understanding of its long term variations is necessary at least to be able to judge the secondary effects as e.g. the secular change in the period, considered by Božić et al. (1995).

Table 2. Log of the Haute Province and Calar Alto observations. The phase and $V_{\rm orbit}$ are calculated in the same way as in Table 1

JD −2 400 000	obs. date[a] month/year	phase	$V_{\rm orbit}$ km s^{-1}
	Hα		
49298.43	CA 11/93	112.508	0.50
49655.42	HP 10/94	115.326	−9.24
49704.34	CA 12/94	115.712	10.11
49707.38	CA 12/94	115.736	10.36
49820.42	HP 04/95	116.628	7.51
49825.42	HP 04/95	116.668	9.05
49836.35	HP 04/95	116.754	10.40
49839.34	HP 04/95	116.778	10.24
49913.42	CA 07/95	117.363	−7.90
	Fe II 5317		
49299.45	CA 11/93	112.516	1.03
49656.35	HP 10/94	115.333	−9.01
49706.43	CA 12/94	115.729	10.31
49820.42	HP 04/95	116.628	7.51
49835.62	HP 04/95	116.748	10.40
	He I 5876		
49302.36	CA 11/93	112.539	2.51
49657.35	HP 10/94	115.341	−8.74
49705.51	CA 12/94	115.721	10.23
49707.42	CA 12/94	115.736	10.36
49824.42	HP 04/95	116.660	8.78
49834.58	HP 04/95	116.740	10.38
50075.42	HP 12/95	118.642	8.08

[a] CA=Calar Alto Observatory; HP=Observatoire de Haute Provence

Our set of HEROS spectra is still very limited in time coverage. Nevertheless, they allow us to check the character of orbital variations in individual lines. Dynamical spectra (phase/time series grayscales) of four selected emission lines are shown in Fig. 1. A detailed inspection of the plots shows what is known already from previous studies, namely that absorption cores of Balmer lines and emissions of Balmer, Paschen, metallic and O I lines follow the orbital motion of the primary. These features are formed in its circumstellar disk. Because our data do not cover the phase of primary conjunction, we can estimate only roughly that the semiamplitude of radial velocities is about 10 km s^{-1} for all these lines. This is well consistent with the value derived for the primary component by Gies et al. (1998) or Božić et al. (1995).

Besides the well known orbital variations, Fig. 1 indicates also a new and important property of emission lines. In all previous studies and also in our 1993–1996 spectra, the emission lines of metals were stable and symmetric (see the dotted profiles of Fe II 5317 and 6318 profiles in Fig. 2). Fig. 1 documents clearly the stronger red component of Balmer and metallic lines and proves the variability of their profiles on a time scale of years. An opposite asymmetry with a slightly stronger blue emission peak can be detected only in the O I 8446 line. However, the effect may result from a blend with the Paschen 18 line. We discuss the most important groups of lines in the next subsections and the possible nature of the long-term variations in Sect. 5.

Table 3. Observations obtained with HEROS. b stands for spectrum in the blue, r in the red channel. The phase and $V_{\rm orbit}$ are calculated in the same way as in Table 1

JD −2 400 000	Frame No.	channel	phase	$V_{\rm orbit}$ km s^{-1}
50826.2890	f0869	r	124.5692	4.38
50841.2487	f0881	r	124.6873	9.60
50846.3028	f0928	r	124.7272	10.29
50850.2611	f0935	b+r	124.7584	10.39
50854.2787	f0950	b+r	124.7901	10.07
50855.2861	f0968	b+r	124.7981	9.93
50856.2424	f0982	b	124.8057	9.77
50856.2407	f0983	r	124.8056	9.77
51029.6990	f0098	b+r	126.1750	−9.26
51045.6095	f0271	b+r	126.3006	−9.88
51053.5823	f0475	b+r	126.3635	−7.87
51064.6631	f0725	b+r	126.4510	−3.16
51066.5895	f0773	b+r	126.4662	−2.20
51086.5497	f0917	b+r	126.6238	7.29
51088.5126	f0976	b+r	126.6393	7.98
51090.5085	f1024	b+r	126.6550	8.60

3.1. Fe II *emission lines*

Up to this study, the Fe II emission lines were considered to be relatively stable and symmetric according to the assumption about their formation in the inner axially symmetric part of the circumprimary disks. However, we could detect a trend toward an asymmetry already in our Ondřejov 1997 spectra. All our 1998–9 spectra show that the line profiles have stronger red components. This is demonstrated both by the dynamical spectra in Fig. 1 and in Fig. 2 showing the profiles for selected Fe II strong unblended emission lines.

Fig. 2 indicates the following qualitative conclusions:

- The profiles are similar for all Fe II emission lines. Thus we assume that any of the strong lines included in the figure can be considered as a representative of the Fe II emission profiles for epochs, when our observations were limited only to a short spectral interval.
- Comparison of the HEROS 1998 spectra and those obtained in previous years indicates strong long-term variations. The symmetric profile observed in Fe II lines in 1993–1997 changed into asymmetric profile with a dominant red component.
- There is no significant difference in the positions of the violet and red emission peaks and their separations for different Fe II lines. The mean separation of the peaks, with the error derived as the statistical error of the mean of values measured for 10 Fe II emission lines, is 303 ± 4 km s^{-1}.
- Comparison of the full line and dotted profile of the Fe II 5317 line proves that the radial velocity of the red emission peak decreased in 1998 with respect to 1993–1996

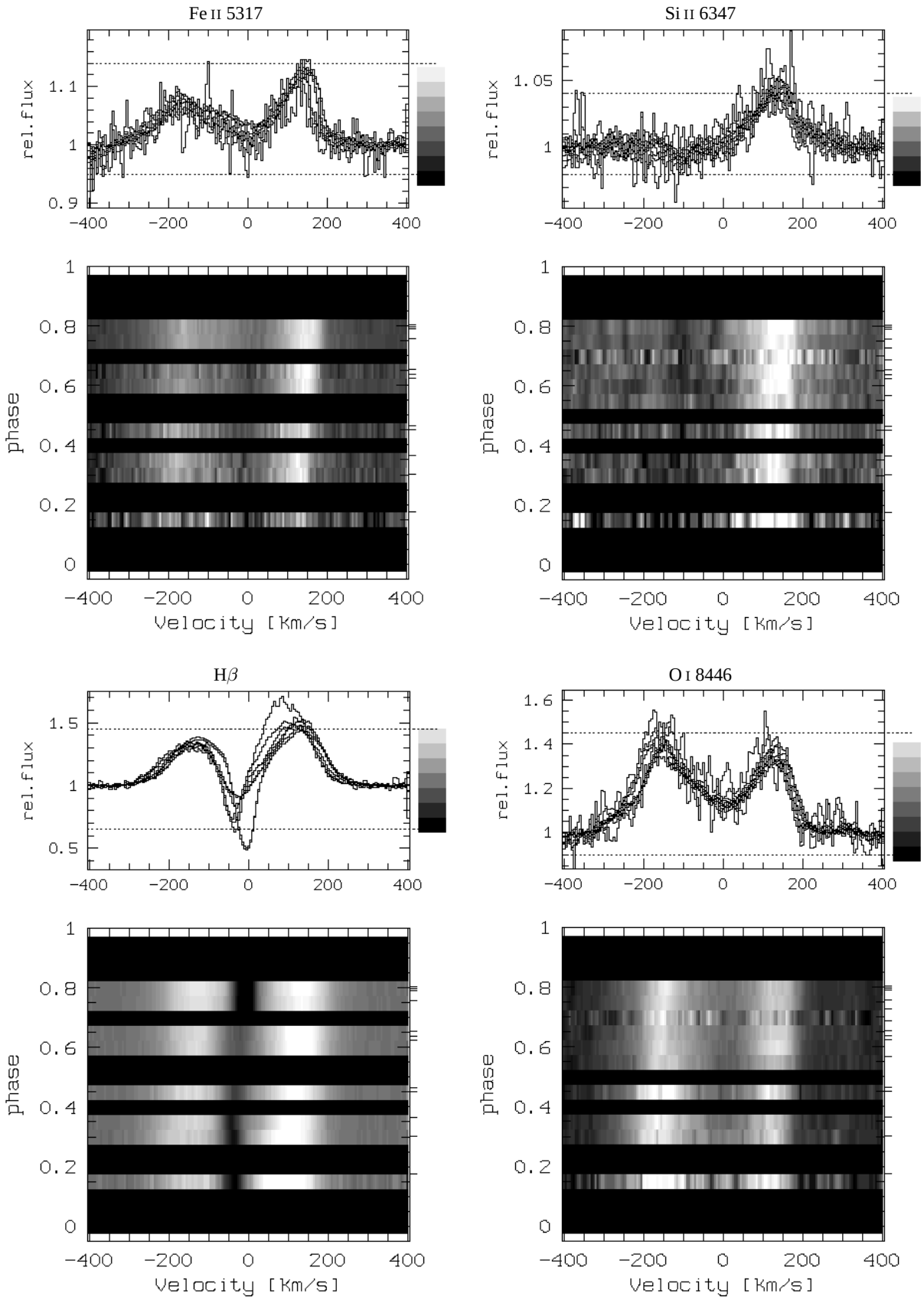

Fig. 1. Phase variations attributed to the primary's Be disk of selected spectral lines in the spectral range of HEROS sorted in 20 phase bins. Tick marks at the right margin indicate the exact phases of the spectra

observations. The RV difference is less significant for the Fe II 6318 profiles.

In order to evaluate quantitatively the long-term Fe II variations, we measured the equivalent width, position of violet and red edge of the lines and intensity of violet and red emission peaks for Fe II 6318 and 6456 and derived their V/R (ratio of maximum fluxes in violet (V) and red (R) emission components). The both lines are relatively weak and can be blended with atmospheric absorption lines. Consequently, the error of an individual EW or RV measurement may reach $\approx$ 10–20 %. The V/R values for Fe II 6318 and 6456 lines plotted in Fig. 3 demonstrate the development of the asymmetric profiles of metallic lines. The trend is well consistent with an increase of polarimetry over the same period (McDavid 1999).

Variations by 10 – 20 % may be present also in the line width and in the equivalent width.

The high resolution emission lines do not exhibit any difference due to different resolutions.

3.2. Balmer & Paschen emission lines

Except for Hα, which also in 1998 shows an approximately symmetric profile and variations, the other Balmer and Paschen emission lines show similar emission asymmetries, i.e. a stronger red peak, as the Fe II lines. Nevertheless, having no data covering other hydrogen lines than Hα before 1998, we can only suppose that this asymmetry developed also in H I during 1997/8. In our 1998 HEROS spectra, V/R is > 1 for Hα but < 1 for Hβ, Hγ, and Hδ.

3.3. He I *emission lines*

In our observations of 1993–1996 (see Fig. 6), He I 6678 shows variations with approximately the same maximum intensity of the blue and red emission components. It is worth comparing dynamical spectra from these seasons (Fig. 6) with those from our HEROS 1998 observations for He I 6678 and 7065 (Fig. 4). In spite of the considerable handicap of data missing at the primary conjunction, the figures indicate a similar although weaker trend in asymmetry of the emission peaks as described for Fe II (see Sect. 3.1) and H I (see Sect. 3.2). The orbital variations in 1998–1999 were asymmetric in the sense that the maximum intensity of the blue emission peak in He I lines was by 3–4% lower than that of the red peak. This small and still tentative effect has two important consequences for modeling of the ϕ Per system:

1. The He I emission profiles show a combination of two kinds of variations: I) the already known orbital variations, II) long term variations of their asymmetry. The latter variations are weak, but of the same character as the unambiguously detected long term variations in the Fe II and H I line profiles.
2. The asymmetry variations of all emission lines (except He II which was not detected in our spectra with insufficient S/N) reflect variations in the same circumstellar structure. Although this conclusion is still preliminary, it is very impor-

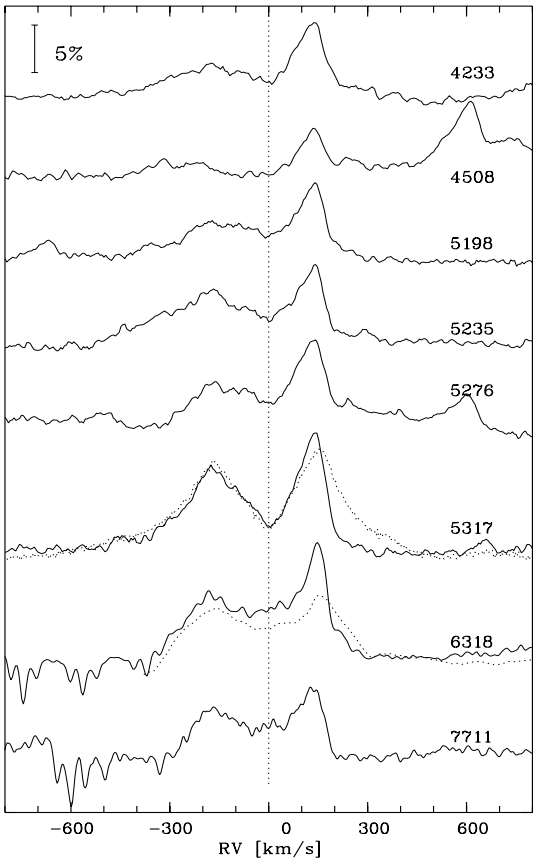

Fig. 2. Examples of Fe II line profiles. Full line profiles are the average of all HEROS spectra obtained in 1998 (see Table 3). The dotted profile of Fe II 5317 is the CA 12/94 spectrum and the dotted profile of Fe II 6318 is the mean of all Ondřejov profiles obtained in 1993–1996

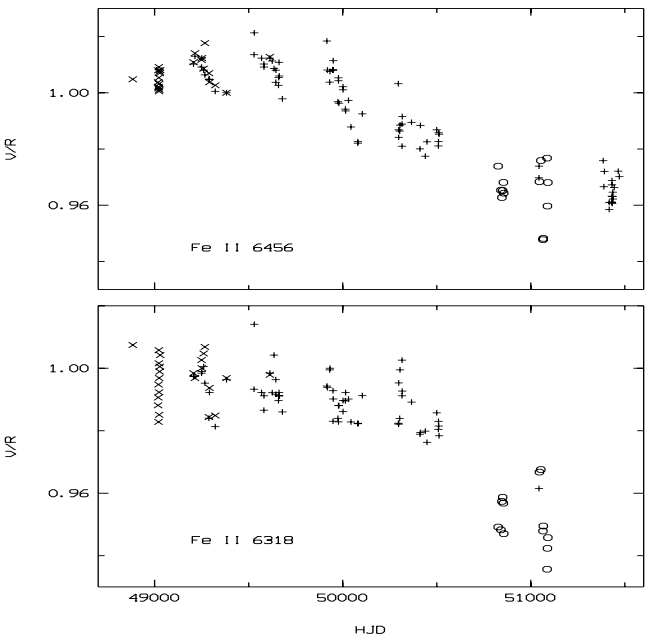

Fig. 3. V/R variations of Fe II 6318 and 6456 lines. + represents spectra from the Ondřejov 2m telescope, ○ from HEROS. x are values measured in Ondřejov spectra used by Božić et al. (1995). Fe II 6318 was outside the observed region in Ondrejov 1999 spectra

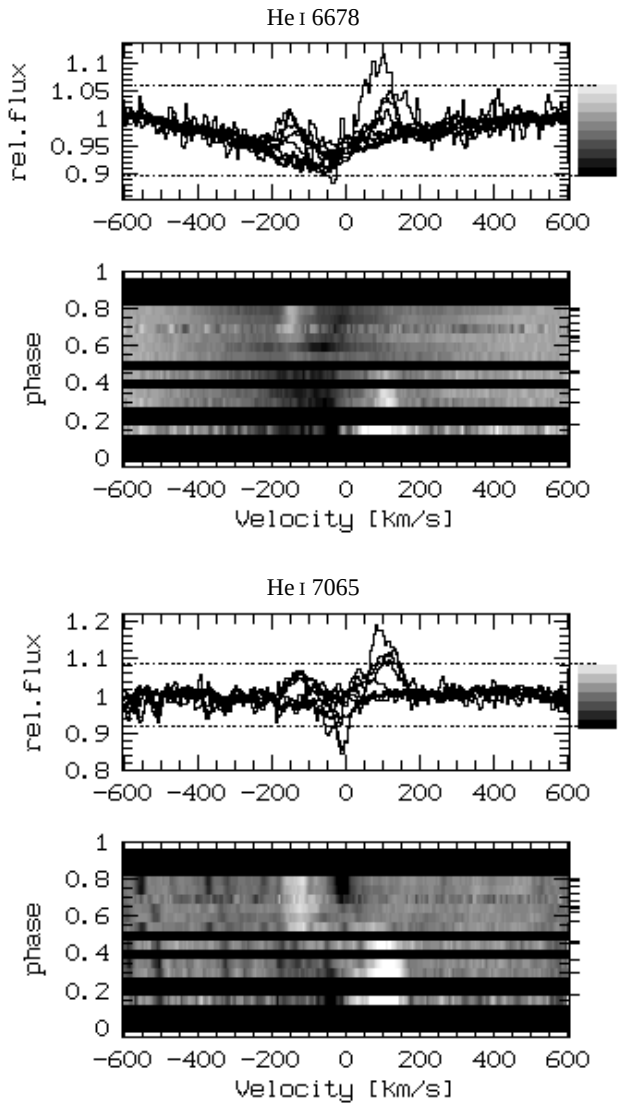

Fig. 4. As Fig. 1, but for the He I emission component

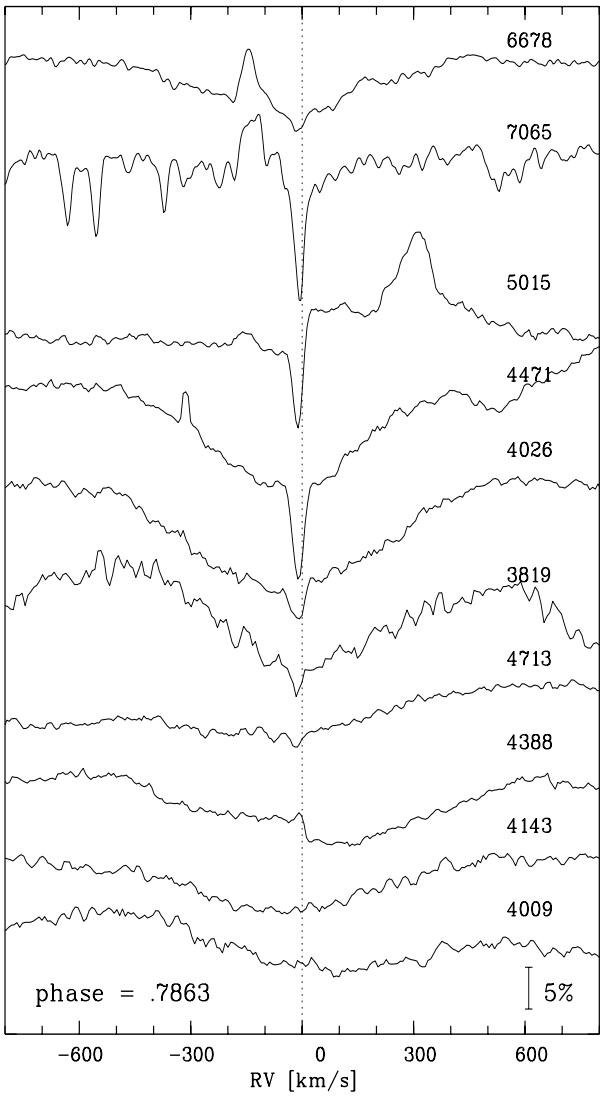

Fig. 5. He I line profiles in the HEROS spectrum f0950 (phase= 0.790). He I 5015 is blended by Fe II 5018, while the apparent step in He I 4388 is caused by the red emission component of Fe II 4385

tant for the interpretation of He I components and for any model of the whole binary system.

4. Detailed analysis of He I lines

The He I lines show many peculiar features which were already pointed out in previous papers. The excellent spectral range of the HEROS spectrograph enables to study the occurrence of special features mentioned in Sect. 1 in individual He I line profiles. Fortunately, part of the HEROS spectra have been obtained during the phases of quadratures. We use them mainly to study the occurrence of He I emission and shell components.

Our present data do not allow to study the orbital variations for many different lines in detail. The whole orbital cycle is covered with a good phase resolution only by the Ondřejov spectra. Their spectral region includes the following lines of sufficient intensity: Hα, He I 6678, Si II 6347, Fe II 6318 and Fe II 6456.

4.1. *Occurrence of* He I *emission and shell components*

Some of the HEROS spectra were obtained at phases, when the He I 6678 emission feature is strongest. They are also suitable for a search for such emission components in other optical He I lines. Our analysis of the HEROS spectra does not fully cover the He I 5875 line, which falls into the gap between the red and blue channel of the Heros spectrograph in four red spectra obtained at phases larger than $0.^P75$. Some of the weak He I lines cannot be recognized due to relatively low S/N and their large rotational broadening.

Fig. 5 shows the selected He I lines at phase $0.^P790$. The lines can be divided in three main groups:

1. Lines showing both emission and absorption shell components - He I 7065, 6678, 5875 (see also Fig. 8), 5015 and 3889. Only a weak shell component appears in He I 6678 (for more detailed analysis see Sect. 4). On the other side,

the emission component is only weak in He I 5015, which is heavily blended with Fe II 5018. He I 3889 is strongly blended with H I 3889 (H8), but comparison with Hϵ and H9 confirms that the shell absorption is due to He I. Emission is present, but the relative contribution of the two lines cannot be disentangled. Both emission and absorption components are strong in the remaining two lines. We looked also for He I 7281.349 (2^1P^0–3^1S), which comes from the same lower excitation level as He I 6678. With the used spectral resolution we cannot decide if the line is extremely weak or whether the absorption line is filled with emission. Neither an absorption nor an emission He I 7281 line was detected in IR studies of He I lines of B-type stars (e.g. Jaschek et al. 1994). Any definitive conclusion about its presence or strength is, however, complicated due to the fact that the line is located in a cluster of telluric water vapor lines. A weak emission bump in He I 4388 (see Fig. 5) can be explained by emission component of Fe II 4385.

2. Lines with only shell component - He I 4471 and 4026, weaker in He I 3819 and 4713 and possibly present in He I 3965 (the whole line is hidden in the blend with Hϵ, but the shell component of He I 3965 can be detected in the blue wing of Hϵ.) All detections of the shell components in our HEROS spectra correspond to the shell attributed to the primary disk by Poeckert (1981). The fact that we were not able to detect the narrow shell lines that Poeckert associated with the circumstellar disk around the secondary component may be due to a lower S/N in the HEROS spectra. As was shown already by Poeckert, the intensity of the components is strongly phase dependent. We can detect the strongest components for phases 0.7–0.8, when they are conspicuous in He I 4471 and 4026 and detectable in He I 3819 and 4713. At phases close to the first quadrature, a weak shell component can be detected only in He I 4471 and 4026.
3. Lines with only photospheric rotationally broadened profiles. We show only He I 4387, 4143 and 4009 lines in Fig. 5. Most of the others, e.g. He I 4923 or 4168 are strongly blended with emission Fe II lines. However, the blends destroy mainly the red wings of He I lines and do not influence detectability of the emission and shell components at the given phases.

For the identification of the site and process of formation of the emission and shell components, it is desirable to find determining transition parameters in each of the above defined groups. Such a link is offered in Table 4. The occurrence of the emission and shell components is well related to atomic transition of the given spectral line.

The following conclusions can be drawn from Table 4:

- The emission component occurs exclusively in the lines coming from transitions between the second and third He I atomic levels. The emission component can be present both in singlet and triplet lines.
- Only the shell component appears in triplet lines excited from the 2^3P^0 level with the energy of 20.87 eV. Both the emission and shell components can be recognized also in singlet lines of 6678 and 5876 Å. The intensity of the shell component decreases for near-ultraviolet lines with the same lower transition level.
- The lines which do not fulfill the above criteria exhibit photospheric rotationally broadened profile.

Table 4. List of studied He I lines and their characteristics.

Wavelength	transition	type	lower level [eV]	upper level [eV]
I. Lines with emission and shell components				
6678.1499	2^1P^0–3^1D	singl	21.13	22.97
5875.7002	2^3P^0–3^3D	tripl	20.87	22.97
5015.6802	$2^1S - 3^1P^0$	singl	20.53	22.99
3888.6460	$2^3S - 3^3P^0$	tripl	19.73	22.91
7065.1899	2^3P^0–3^3S	tripl	20.87	22.62
II. Lines with a shell component				
4471.4771	2^3P^0–4^3D	tripl	20.87	23.63
4026.2000	2^3P^0–5^3D	tripl	20.87	23.94
3819.6060	2^3P^0–6^3D	tripl	20.87	24.11
4713.2002	2^3P^0–4^3S	tripl	20.87	23.49
III. Only photospheric line profile				
3964.7270	$2^1S - 4^1P^0$	singl	20.53	23.64
3926.5300	2^1P^0–8^1D	singl	21.13	24.27
4009.2700	2^1P^0–7^1D	singl	21.13	24.21
4120.9930	2^3P^0–5^3S	tripl	20.87	23.87
4143.7588	2^1P^0–6^1D	singl	21.13	24.11
4168.9712	2^1P^0–6^1S	singl	21.13	24.09
4387.9282	2^1P^0–5^1D	singl	21.13	23.94
4921.9292	2^1P^0–4^1D	singl	21.13	23.63
5047.7388	2^1P^0–4^1S	singl	21.13	23.57

One may suspect a weak emission in the red wing of He I 4471 in Fig. 5. The effect is at least partly caused by imperfect automatic normalization. We checked that no phase variations appear in this region and so we can exclude any emission similar to those in the lines listed in the first block of Table 4.

4.2. *Phase variations of* He I *6678 emission component*

The results of Sect. 4.1 indicate that the emission and shell components are connected with a different way of excitation and may be formed in different parts of the circumprimary disk. Therefore, it is simplest to start modeling the two features separately and only in lines in which only one of the features is dominant. Of the five He I lines with emission component, He I 6678 fulfills this condition best. It shows a strong emission but only a weak shell component.

Taking into account the long-term variations in 1997–1999, (see Sect. 3) we derived the phase-averaged He I 6678 profiles only from our 1993–1996 Ondřejov spectra and discuss them below.

The orbital variations of the He I 6678 emission component can be seen in the dynamical spectrum in Fig. 6, upper panel. The spectra are averaged in every phase bin of the width of

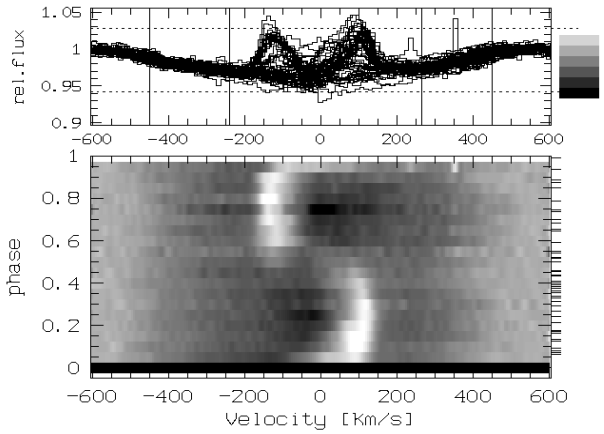

Fig. 6. Dynamical spectrum of He I 6678 (lower panel). The spectra are averaged in 20 phase bins, radial velocity step is 5 km s^{-1}. The individual profiles are overplotted in the upper panel. The full lines mark the range of the stable pseudo-photospheric profile (see Sect. 3)

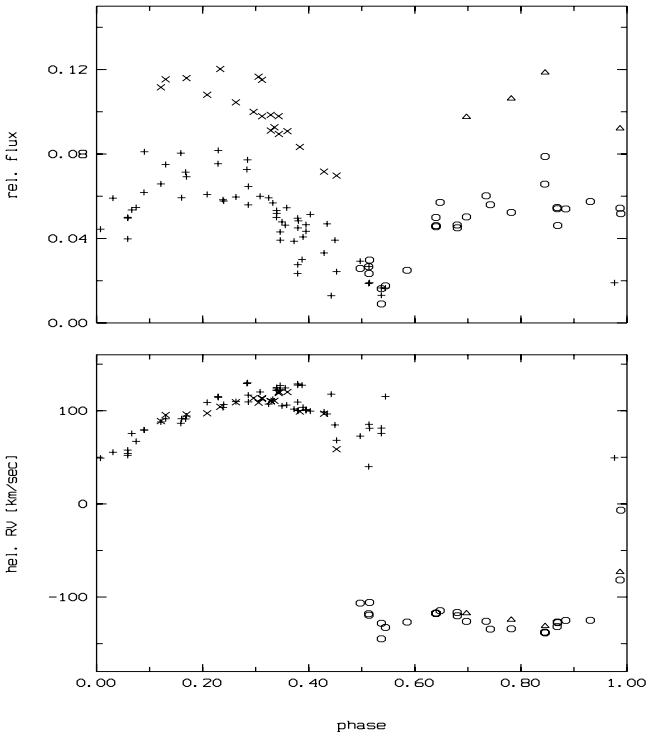

Fig. 7. Relative intensity (upper panel) and radial velocity (lower panel) of the He I 6678 emission component. The circles and crosses correspond to the "violet" and red component, respectively. x and △ represent the same quantities in spectra used by Božić et al. (1995)

$0.^P05$. In the gray-scale representation, the bright part of the figure corresponds to the emission component.

In order to isolate profiles of the emission component for the analysis and modeling, we need to subtract a template photospheric profile of the primary star. Because we found no satisfactory agreement of the observed profiles with the computed synthetic ones, we decided to construct the profile - as did Gies et al. (1993) - in a purely empirical way. Both lower and upper panel of Fig. 6 indicate that the photospheric profile is constant in the wings over the whole orbital cycle. Variations are observed in its central part convolved with the obviously variable emission component. We are not able to distinguish any small variations in the core of the absorption photospheric profile or in the emission component. We assume that the photospheric profile is constant over the whole orbital cycle and that it is identical with the mean profile out of the region, where the emission component appears. These limits are indicated by vertical lines in the upper panel of Fig. 6. We used polynomial regression to fit a polynomial of the fifth degree to the parts of the line wings in the interval (-490,-240) and (265,455). These limits were fixed again empirically. The combined polynomial in the interval (-240,265) and the mean profile out of this interval was used as the template photospheric profile. We derived the difference emission components by subtracting the template absorption profile.

As the main characteristics of the emission components, we measured their radial velocity and intensity. The results are shown in Fig. 7. Taking into account the fact that at some phases we can observe both the violet and red component of the emission profile and in order to avoid any assumption about their origin, we show the parameters of the both components by different symbols. The following conclusions can be drawn from the figure:

- Both V and R emission components can be observed simultaneously only in a narrow phase interval near $0.^P5$. At these phases, their intensity is reduced to less than one third of the maximum intensity.
- Radial velocity of the both components, derived by fitting the Gaussian, shows much flatter distribution than can be expected for sinusoidal orbital variations. The R component shows an inconspicuous maximum of 115 km s^{-1} at phase $0.^P30$. However, even for the phases close to $0.^P5$, its radial velocity does not decrease under $\approx$ 50 km s^{-1}. The V component shows even a shallower minimum of -138 km s^{-1} close to $0.^P8$ and -instead of decrease for lower phases- the data indicate a weak secondary minimum of -135 km s^{-1} at $\approx 0.^P55$.
- While both the amplitude and shape of the RV curve of emission components seem to be stable on a time scale of years, their intensity is strongly variable. It is almost twice in 1991–1993 (spectra by Božić et al. 1995) than in 1993–1999.

Particularly the second item contains the significantly new property of the He I emission components, which is hardly consistent with a model in which one or both components are formed in a thin envelope close to the secondary star - compare the lower panels of Fig. 7 and Fig. 4 in Gies et al. (1993).

4.3. He I *5876 and 7065 phase variations*

Fortunately, our observations of He I 5876 and 7065 are collected close to the phases of quadratures and secondary con-

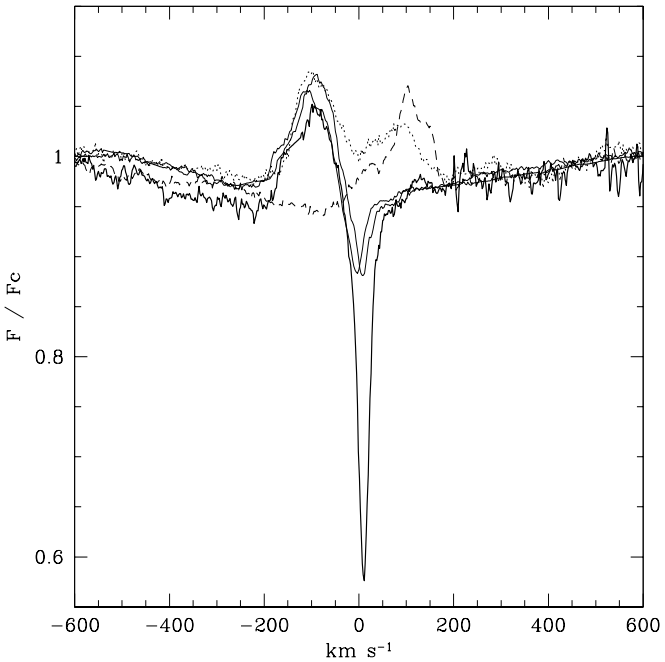

Fig. 8. High resolution He I 5876 emission lines at orbital phases 0.341 (dashed), 0.539 (dotted), 0.721 (solid), 0.736 (solid) and 0.740 (solid, bold)

junction and both lines were covered by HEROS with sufficient sampling to derive some general properties. A detailed comparison of He I 6678, 5875, and 7065 in phases when these lines are available proves that the phase variations of their emission components follow the same pattern. It is very probable that the difference in the shell component (see Sect. 4.4) is partly either due to different spectral resolutions or to cycle-to-cycle variations. E.g. the HEROS spectrum f0475 taken at cycle 126.36 shows a strong shell absorption, while OHP data from cycle 115.34 show no absorption at all for He I 5876.

The fine structure in the emission profiles of He I 5876 is also illustrated in Fig. 8. Striking features are the 'outer' emission bumps at quadratures, which always develop in the wing of the stronger emission component and which are symmetric in phase. No similar bumps develop at $0.^P54$. This causes us to suggest that the emission region is rather symmetric with respect to the symmetry axis through L_1.

Another point is that the emission edges at quadratures match those at inferior conjunction. We interpret this result as a unique maximum kinematic broadening of the He I emission region.

The velocity of the He I 5876 main peak coincides with the main peak of the He I 6678 emission feature. Gies et al. (1998) found a secondary peak at a lower velocity only resolved near quadrature. This secondary peak is not resolved in our data for 6678. Our high resolution spectra for He I 5876 show a striking bump in the high velocity wing of the main emission component; only at $0.^P341$ there are traces of a secondary peak on the low velocity wing as it occurs in He I 6678 (See Fig. 8).

Provided that the Gies et al. (1998) model is valid, we may interpret the weak and the strong emission features as physical components, where the strong peak originates in the disk around the companion star and the weak component either in the disk around the primary facing the secondary or between the two disks near L_1, we can easily estimate the expected line profile shape at the primary conjunction, when the kinematic broadening due to the orbital motion can be neglected. We would expect a line profile where the strong and the weak emissions are at velocity zero and the FWHM is nearly that of the broadest of the two emission components. However, the fully resolved double peak He I 5876 profile at $0.^P54$ (dotted profile in Fig. 8) does not agree with the expected profile shape.

If all emission originates in a large area of the circumprimary disk facing the secondary; e.g. one half or one third of the circumprimary disk, we would expect double peak profiles of half intensity near $0.^P5$ and $0.^P0$ and asymmetric fractional profiles at any other orbital phase (see Fig. 10).

4.4. He I *shell component*

Due to the limited number of our spectra covering lines with the shell component, we cannot study their phase dependent properties in detail. Nevertheless, we can make some statements which bear on the binary model.

The radial velocities of the shell lines were determined by fitting Gaussians to the line centers. The measured values are plotted in Fig. 9. The figure shows significant phase variations with a maximum approximately at $0.^P8$, minimum at $0.^P4$ and full amplitude of 40 km s^{-1}. These variations are well consistent with those of H I shell lines measured by Božić et al. (1995) (see their Fig. 5).

Our observations agree with those of Poeckert, who observed strong shell components at the time of primary conjunction ($0.^P0$) and weaker shell components at the quadrature. Comparison of Poeckert's and our data both around quadrature indicates that the shell components (e.g. in He I 4471) might be stronger in 1993–1998 than in 1976–1979. The effect can be, however, partly explained by different spectral resolution of the both data sets.

Phase variations of the shell component can be also followed in Fig. 8. The strongest shell line at $0.^P74$ is collected at a spectral resolution of $\Delta V = 6$ km s^{-1}; the other two lines at $0.^P736$ and $0.^P721$ are observed one cycle earlier with $\Delta V = 9$ km s^{-1}. Note that they are consistent with the thermal broadening of He at $T = 10\,000$ K (≈ 6.4 km s^{-1}).

The convolution of the highest resolution profile with the instrumental profile of the lower-resolution shell profiles clearly shows that the difference in shell intensity can partly be caused by their different spectral resolutions. This means that only the $0.^P740$ shell component is fully resolved. Contrary to the He I 6678 shell components observed by Poeckert (1981), no additional weak shell component is visible in our He I 5876 profiles.

There are two strong reasons why the He I shell component is likely to originate in circumstellar matter around the primary.

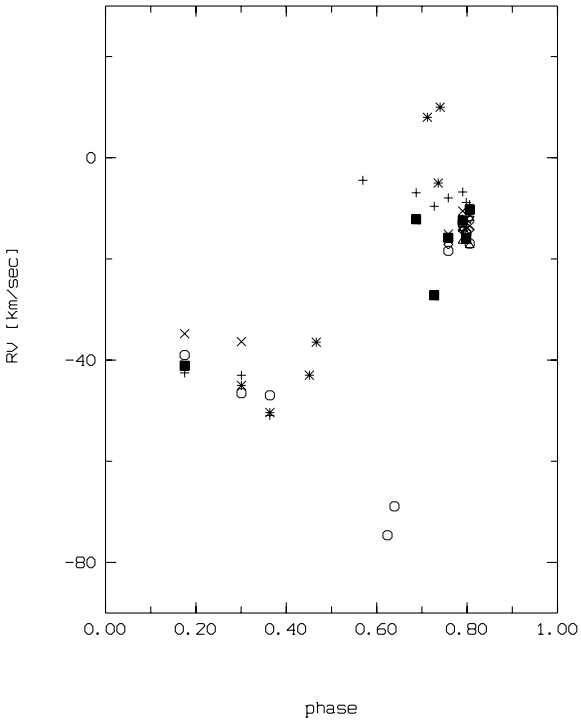

Fig. 9. Radial velocities of He I shell components. Components measured in different lines are plotted with the following symbols; He I 7065 +, 6678 ■, 5875 ∗, 5015 ○, 4713 △, 4471 ×, 4026 ◇, 3819 ⋆

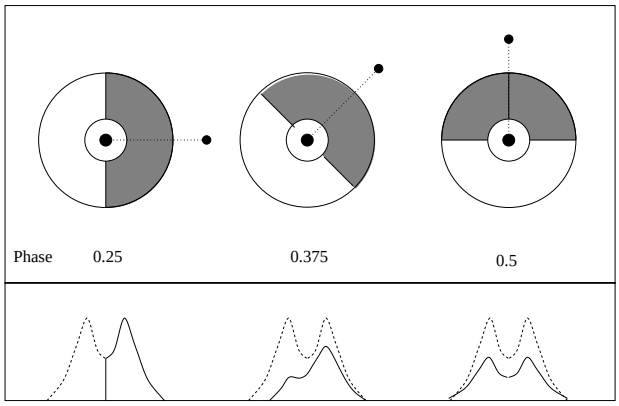

Fig. 10. Sketch of the He I emission region as a fraction of a Keplerian disk facing the secondary and the corresponding shape of the emission line. The dashed profile is for optically thin emission from the whole axisymmetric disk. For $0.^P25$ only the receding part of trajectories contribute to line emission resulting in a half profile. For $0.^P5$ both receding and approaching parts of the disk contribute by equal amount to the line profile, hence a symmetric double peak at half intensity results. For $0.^P375$ only one quarter of the approaching disk part contributes to the blue part of the profile, while three quarters of the receding disk side contributes to the stronger red peak

First, the shell profile ($I_{\rm sh} = 0.58F_c$) is deeper than the continuum flux contribution by the secondary in the optical ($\simeq 4\%$; Poeckert 1981) and second, the radial velocity of the shell profile is much closer to and in phase with the primary motion ($K_1 = 9.47\,\mathrm{km\ s^{-1}}$) than to the RV amplitude of the secondary ($K_2 = 81.3\,\mathrm{km\ s^{-1}}$), which should reach maximum at the quadrature. No narrow shell components to be attributed to the secondary's orbit could be detected in our spectra.

5. Discussion

Gies et al. (1993) interpreted the emission components in He I 6678 as two independent features that keep their identity during the whole orbital cycle. This leads naturally to the interpretation in which the two components are formed in different parts of the binary system. One of the observational consequences of that model would be a smooth variability of radial velocity of both components, similar to radial velocity curves of binaries. However, Fig. 7 shows a rather different and discontinuous character. Smooth variations can be seen in the intensity of the stronger component (the faint component is spectroscopically not resolved in our Ondřejov data), but its radial velocity stays outside the interval (-20 ± 60) km s^{-1} even at phases close to $0.^P5$. This result is not consistent with an interpretation that only one of the components is formed in the disk around the primary and the second one in the disk around the secondary. It stimulated us to search for and model a single process that produces both He I emission components.

We cannot, however, confirm the model, in which all He I emission is formed in the disk around the secondary star (Božić et al. 1995). The indicated similar character of long term variations of emission He I components (superimposed on the orbital phase variations) as in Fe II emission lines, consistent phase variations of their V and R components, their radial velocities and fine profile structure support the idea that both He I emission components are formed in the same part of the binary system, which does not follow closely the orbital motion of either of the stars.

The analysis of high resolution He I 5876 line variations also supports the idea of a pure illumination effect in the axisymmetric disk around the primary. Each profile resembles a fraction of a symmetric double peak profile. This can be qualitatively explained if the radiation of the secondary excites not the whole disk but only its closest part.

In a series of papers, Smith et al. (1997 and references therein) argue that He I 6678 emission of single Be stars (and in particular of λ Eri) originate very close to the star in the upper layers of the photosphere, where the He I resonance singlet λ584 becomes transparent by the so-called Auer-Mihalas process.

An important constraint for the He I excitation mechanism working in ϕ Per is the observational fact that the main kinematical broadening of He I 6678 and He I 5876 emission does not exceed $V = 210\,\mathrm{km\ s^{-1}}$ at any orbital phase (Figs. 6 and 8), hence the He I emission must originate beyond $R \simeq 5R_*$ in the circumprimary disk as concluded by Hummel & Vrancken (1995). We suppose that the central star is very unlikely the source of the He I in ϕ Per, instead it seems more likely the secondary to be responsible for the He I emission.

A direct application of the classical ionization theory to the ϕ Per binary system in order to prove the ionization in the cir-

Table 5. Comparison of emission line strength of He I lines observed in ϕ Per, γ Cas and those predicted by the classical ionization theory

λ[Å]	EW$_\phi$	flux$_\phi$	I_ϕ	flux$_\gamma$	I_γ	I_o
7065.1899	−120	0.635	2.05	0.662	1.43	0.42
6678.1499	−50	0.742	1.00	0.735	1.00	1.00
5875.7002	−70	0.910	1.72	0.916	3.00	3.50
5015.6802	−20	1.134	0.62			0.76

flux$_\phi$, flux$_\gamma$: continuous flux distribution with respect to flux at 550 nm for ϕ Per (Goraya 1984) and γ Cas (Goraya 1980), respectively
I_ϕ: observed emission strength = EW$_\phi$ * flux relative to that in He I 6678 for ϕ Per
I_γ: as I$_\phi$, but derived for γ Cas (unpublished HEROS data)
I_o: Osterbrock's ratios for T_{gas}=10 000 K, $N = 1.10^6$ cm^{-3}

cumprimary disk is hardly possible because the basic assumptions are not fulfilled. One has to consider two facts, which would make any quantitative estimate misleading: I) the density in the disk is not constant but increases by several orders both towards the primary and towards the disk equator, and II) the geometrical distribution of the gas in the disk is very different from isotropic with respect to both the primary and secondary star. Without an exact modeling we can add only very limited qualitative justification.

A very rough estimate of the Strömgen H^+ radius around the primary B0.5 star gives a thickness of the ionized layer only of a few hundreds of the primary radius. The He^+ Strömgen radius is even about a factor 4 smaller. Although the ionization radius will be somewhat larger due to the disk geometry, this is certainly not consistent with the observations indicating the formation of the emission several stellar radii from the primary component. On the other side, a hot star of 53 000 K has its maximum flux close to 500 Å and emits about 2.3 times more photons (ratio of $R_{s,0}$ values) for ionization. The penetration depth of the He^+ equals to that of hydrogen since $T_{\rm eff}$ of the secondary exceeds 40 000 K (Osterbrock 1989). Since there is almost no material between the secondary and the outer edge of the disk, these photons are only geometrically diluted, but not absorbed as in the classical concept of the Strömgren sphere. Therefore not the Strömgren radius but the penetration depth of the ionizing radiation restricts the ionization of the outer part of the circumprimary disk.

We can suppose that the circumprimary disk, which is illuminated by the hot secondary star, is a good candidate for formation of the emission. The exact shape of the excited region depends on the disk density distribution. The effects of geometrical parameters on the resulting emission profiles will be discussed in Paper 2.

For the emission components in the four He I lines, their emission EW and line strength ratios are collected in Table 5. For comparison, we include the analogous emission characteristics derived from He I lines of the well known B0.5IVe star γ Cas, observed with HEROS in 1996. Comparable emission strengths for ϕ Per and γ Cas indicate that the excitation mechanism is the same in both stars. There is no evidence for binarity in γ Cas and we can assume that its inner disk -similar as in other Be stars- is excited mainly radiatively. However, the ϕ Per emission components are formed further from the primary star, where the radiative field of the secondary star is more effective. The poor agreement between the predicted and observed ratio - particularly for He I 7065 and 5876 - can be partly explained by a large difference in corresponding densities. It may also indicate that the emission is connected not only to the ionization but also to a kind of fluorescence, i.e. excitation by strong lines in the UV region. Another argument for such a process is that the emission is not observed in all He I lines as one would expect for complete ionization and subsequent cascade transitions. The selection effect described in Sect. 4.1 might be explained if only selected energy levels are populated by the UV fluorescence. Although one could speculate about concrete transitions, the detailed modeling requires an exact solution of equations of statistical equilibrium and is beyond the scope and aim of this paper.

The difference between the binary parameters derived by Božić et al. (1995) and Gies et al. (1993) can be well explained provided that the basic assumption by Božić et al., who identified the He I emission with the secondary component, is not correct.

One of the new findings presented in this paper is the discovery of long term V/R variations in most of the emission lines, which started after 1996 (see e.g. Fig. 3). They are most pronounced in Fe II emission lines in our 1998–1999 spectra. A further inspection of the OHP and Calar Alto data shows no significant line asymmetry before 1996. The Fe II line profiles in 1998–9 are indistinguishable from asymmetric line profiles as they occur in long term variable single Be stars. These variations are interpreted as global oscillations in the disks (Okazaki 1991, 1997). Although our data do not cover the whole cycle of Fe II V/R variations, we can very roughly estimate the quasi-period. The September–October 1999 points in Fig. 3 seem to be obtained about at the V/R minimum. Provided that the variations are sinusoidal, we can estimate that the quasi-period is at least 4000 days, or 11 years. Such a period is well consistent with periods of V/R variations (global oscillations) in single Be stars (e.g. Okazaki 1997). This probably means that we accidently monitored a growing large scale density perturbation in ϕ Per.

The above suggested presence of global oscillation that may coexist with the orbital processes, should be taken into account when determining the basic orbital parameters or at least their accuracy. Depending on the method of RV determination of emission lines, their RVs can be little influenced by the variable emission profile. We do not assume that the accuracy of Božić's et al. period is decreased by this effect. Most of their data were taken at the time when the emission lines were symmetric and constant. However, ϕ Per shows a potential risk of using the circumstellar emission lines in determination of orbital parameters.

Unlike the cataclysmic variables, in which disk perturbations in the accretion disk are induced by the orbiting hot spot varying with binary phase, the orientation of the density perturbation pattern in ϕ Per is independent of the orbital phase.

The fact that the orbital variations of emission He I profiles became asymmetric after 1996 shows that the growing density pattern has reached the He I excitation region. This scenario makes ϕ Per very exceptional, since the illumination effect in He I, most probably caused by the secondary, can be used to scan the structure and evolution of the global disk oscillation in more detail.

The comparison between Figs. 4 and 6 demonstrates how the long term trend after 1996 influences the phase diagrams. At phase $\simeq 0.2$ the He I line becomes stronger in 1998. The He I emission provides information about the outer part of the disk. We conclude that the high density region of the global density perturbation pattern is located in the receding part of the rotating He I excited sector, which is closer to the observer (it is in front of the connecting line of the binary components). We expect that the precession of the density pattern will cause the stronger emission lines to appear at different orbital phases in the coming years.

ϕ Per may be the first representative of a Be binary system with a hot companion and an anisotropically excited circumprimary disk. Very similar spectroscopic variations were recently reported and analogous binary and disk model suggested for 59 Cyg by Rivinius & Štefl (2000).

6. Conclusions

Our analysis of new ϕ Per spectra brought two new findings, which make this system even more interesting for follow-up studies focused on its Be star disk, both from the point of view of its structure and of the radiative processes in it:

- We argue that the whole He I emission (both V and R components) is formed in the outer region of the circumstellar disk around the primary Be star, which is illuminated and radiatively excited by the hot O-type companion. A detailed modeling of this effect will follow in Paper 2.
- The asymmetry in most of emission lines appearing only during the last three years is connected with a global density pattern conspicuous in the inner region. This pattern is still detectable in the outer disk regions where its effect is combined with the radiative influence of the secondary star in He I line profile variations.

A more detailed investigation of both aspects is planned for our future studies.

Acknowledgements. This work was supported by the Deutsche Forschungsgemeinschaft (436 TSE 113/19) and Academy of Sciences and Grant Agency of the Czech Republic (436 TSE 113/19, 202/97/0326). We thank M. Vrancken and R.W. Hanuschik who kindly obtained the HP 04/95 observations, the referee M.A. Smith for his constructive criticism and corrections of the manuscript, I. Hubeny and K. Butler for valuable comments and suggestions on the He I excitation mechanism, P. Harmanec and P. Koubský for stimulating comments on the manuscript and the second unknown referee for very careful language corrections. We also thank H. Božić and his coauthors who gave their spectra to our disposal, and D. Korčáková, P. Škoda and M. Šlechta, who obtained some of the latest spectra used in this study.

References

Božić H., Harmanec P., Horn J., et al., 1995, A&A 304, 235
Gies D.R., Willis C.Y., Penny L.R., et al., 1993, PASP 105, 281
Gies D.R., Bagnuolo W.G., Ferrara E.C., et al. 1998, ApJ, 493, 440
Goraya, P.S., 1984 A&A 138, 19
Goraya, P.S., 1980, ApJS 73, 319
Harmanec P., 1988, BAI Czech 39, 329
Hummel W., Vrancken M., 1995, A&A 302, 571
Hummel W., Vrancken M., 2000, A&A (submitted)
Jaschek M., Andrillat Y., Houziaux L., et al., 1994 A&A 282, 911
Kaufer A., 1998, Variable circumstellar structure of luminous hot stars: the impact of spectroscopic long-term campaigns, In: Schielicke E. (ed.)Rev. in Mod. Astron. No. 11, p. 177
Ludendorff H. 1910, Astron. Nachr. 186, 17
McDavid D., 1999, PASP 111, 494
Okazaki A.T. 1991, PASJ 42, 75
Okazaki A.T. 1997, A&A 318, 548
Osterbrock D.E., 1989, Astrophysics of Gaseous Nebulae and Active Galactic Nuclei, Mill Valley, University Science Books
Perryman M.A.C., 1997, The Hipparcos and Tycho Catalogues, ESA SP-1200, Noordwijk: ESA/ESTEC
Poeckert R., 1981, PASP 93, 297
Quirrenbach A., Bjorkman K.S., Bjorkman J.E., et al. 1997, ApJ 479, 477
Rivinius T., Štefl, 2000, In: Smith M., Henrichs H., Fabregat J. (eds.) IAU Coll. 175, (in press)
Smith M.A., Cohen D.H., Hubeny I., et al., 1997, ApJ 481, 467
Stahl O., Kaufer A., Wolf B., et al., 1995, J. Astron. Data 1, 3, on CD-ROM
Štefl S., 1999, In: Wolf B., Fullerton A., Stahl O. (eds.) IAU Coll. 169, p. 24
Štefl S., Rivinius Th., 2000, In: Smith M.A., Henrichs H., Fabregat J. (eds.) IAU Coll. 175, (in press)
Suzuki M., Kogure T., Mon M., 1997, In: ASP-CS 130, p. 209
Thaller M.L., Bagnuolo W.G., Gies D.R., et al., 1995, ApJ 448, 878
Vanbeveren, D., Van Rensbergen, W., De Loore, C., 1998, The brightest binaries, Boston: Kluwer Academic Publishers, (Astrophysics and space science library; v. 232), p. 202